International Journal of Biological Macromolecules 297 (2025) 139819

Contents lists available at ScienceDirect

International Journal of Biological Macromolecules

journal homepage: www.elsevier.com/locate/ijbiomac

Development of a StIW111C-based bioresponsive pore-forming conjugate for permeabilizing the endosomal membrane

Felipe A. Escalona-Rodriguez [a,b], Javier La O-Bonet [a,b], Lidia Priscila Ferrer Tasies [c], Karthikeyan Subbarayan [d], Ada L. Rivero-Hernández [a,b], Maricary Sifontes-Niebla [a,b], Alexis Manso-Vargas [e], Luisa De Cola [f], Nora Ventosa [h,i], Belinda Sánchez [e], Carlos Alvarez [a,b], Daniel G. Rivera [a,j], Barbara Seliger [d,g,*], María E. Lanio [a,b,**]

[a] Center for Protein Studies, Faculty of Biology, University of Havana (UH), 25th Street, corner to J Street. Square of Revolution, Havana 10400, Cuba
[b] NanoCancer, Molecular Immunology Center (CIM), 216 Street, corner to 15 Street, Playa, Havana 11600, Cuba
[c] Nanomol Technologies S.L., 08193 Cerdanyola del Vallès, Spain
[d] Institute for Medical Immunology, Martin-Luther University Halle-Wittenberg, Magdeburger Str. 2, 06112 Halle, Germany
[e] Immunobiology Division, Molecular Immunology Center (CIM), 216 Street, corner to 15 Street, Playa, Havana 11600, Cuba
[f] Institute of Supramolecular Science and Engineering, 8 allée Gaspard Monge, BP 70028, 67083 Strasbourg Cedex, France
[g] Institute of Translational Immunology, Brandenburg Medical School, Gertrud-Piter-pLatz 7, 14770 Brandenburg an der Havel, Germany
[h] Institut de Ciència dels Materials de Barcelona, ICMAB-CSIC, 08193 Cerdanyola del Vallès, Spain
[i] Centro de Investigación Biomédica en Red de Bioingeniería, Biomateriales y Nanomedicina, Instituto de Salud Carlos III, Madrid, Spain
[j] Laboratory of Synthetic and Biomolecular Chemistry, Faculty of Chemistry, University of Havana, Havana 10400, Cuba

ARTICLE INFO

Keywords:
Sticholysins
Pore-forming proteins
Non-viral delivery system

ABSTRACT

Gene expression manipulation is pivotal in therapeutic approaches for various diseases. Non-viral delivery systems present a safer alternative to viral vectors, with reduced immunogenicity and toxicity. However, their effectiveness in promoting endosomal escape, a crucial step in gene transfer, remains limited. To address this drawback, we developed a reducible conjugate combining the StIW111C mutant of Sticholysin I, a pore-forming protein, with a polylysine peptide. This conjugate aims to enhance plasmid DNA (pDNA) release from endosomes, thereby improving gene expression. A 16-polylysine peptide was attached to StIW111C via a disulfide bridge to block its membrane-binding site, enabling controlled modulation of pore-forming activity in response to a reductive environment. This modification also enhances the conjugate's positive charge, facilitating binding to nucleic acids. Formation of positively charged nanometric complexes was achieved by mixing pDNA with the bio-responsive StIW111C conjugate and polylysine peptide. In vitro assays showed the conjugate could permeabilize endosomes, but reporter gene expression was limited, likely due to the largest complexes or aggregates that reduced conjugate entry and blocked nucleic acid release. CryoTEM imaging revealed the presence of small aggregate fraction, highlighting the need for further redesign to prevent aggregation and optimize endosomal release of non-viral systems for enhanced gene expression.

1. Introduction

The endosomal escape process has been identified as one of the major bottlenecks for reaching an efficient non-viral chemical-based delivery system [1,2]. The internalized complexes by endocytosis must overcome the *endo*-lysosomal barrier before being degraded by the hydrolytic enzymes in these compartments. Several molecular species have been used to mediate endosomal escape through different mechanisms. Various pH-sensitive amphipathic peptides and lipid molecules disrupt and/or fuse with the endosomal membrane as well as some cationic

* Corresponding author at: Institute for Medical Immunology, Martin-Luther University Halle-Wittenberg, Magdeburger Str. 2, 06112 Halle, Germany.
** Correspondence to: M. E. Lanio, Center for Protein Studies, Faculty of Biology, University of Havana (UH), 25th Street, Square of Revolution, Havana 10400, Cuba.
E-mail addresses: felipe@fbio.uh.cu (F.A. Escalona-Rodriguez), lferrer@icmab.es (L.P.F. Tasies), karthik.subbarayan@uk-halle.de (K. Subbarayan), ada.rivero-hernandez@biophys.mpg.de (A.L. Rivero-Hernández), luisa.decola@unimi.it (L. De Cola), ventosa@icmab.es (N. Ventosa), belinda@cim.sld.cu (B. Sánchez), calvarez@fbio.uh.cu (C. Alvarez), barbara.seliger@uk-halle.de (B. Seliger), mlanio@fbio.uh.cu (M.E. Lanio).

https://doi.org/10.1016/j.ijbiomac.2025.139819
Received 26 June 2024; Received in revised form 10 January 2025; Accepted 10 January 2025
Available online 13 January 2025

polymers, such as polyethyleneimine (PEI), that cause endosome disruption due to the so called "proton sponge effect" [3].

Additionally, pore-forming proteins (PFPs) or peptides have been used to destabilize the endosomal membrane allowing endosomal content to escape into the cytosol. Melittin (pore size: 8.7 nm) [4–6], Listeriolysin O (LLO) (pore size: 40 nm) [7–9], Perfringolysin O (pore size: 25 nm) [10,11], and Diphtheria toxin T domain (pore size: 1.8 nm) [12,13] significantly increased transfection efficiency in vitro when incorporated into non-viral delivery systems. Despite the mechanism by which these polypeptides can mediate the endosomal escape of these complexes is not clearly understood, the pore size of the polypeptide seems to have little influence on the endosomal escape. The proteins or peptides mostly used have some type of regulation of their pore-forming activity either naturally, as in the cases of LLO and the T domain of Diphtheria toxin whose activity depends on pH [14,15], or artificially, that is, through modifications that condition the functionality of the protein or peptide to the presence of certain stimuli in the microenvironment, for example, the reductive potential [4,6,11,16].

Sticholysins (2 isoforms: StI and StII) are PFPs produced by the sea anemone *Stichodactyla helianthus* [17]. They share some characteristics such as a high isoelectric point, a molecular mass of approximately 20 KDa, they are cysteinless proteins, and have a predominantly β-sheet organized structure [18]. These molecules also exhibit high permeabilizing activity, which arises from the formation of hydrodynamic pores, approximately 2 nm in diameter, in membranes containing sphingomyelin (SM) [19,20], a common eukaryotic cell membrane phospholipid.

StIW111C contains a cysteine residue replacing the tryptophan 111. This position is found in the membrane binding site and is one of the most exposed residues on the protein surface [21]. StIW111C readily dimerizes probably due to the high reactivity and degree of solvent exposure of this cysteine residue. Both the monomeric and dimeric variants can lyse human erythrocytes. Nonetheless, the dimeric variant demonstrates significantly lower activity, as evidenced by its approximately 193 times higher concentration required to achieve 50 % hemolysis compared to the monomer [22]. Therefore, binding a large molecule via a disulfide bridge to StIW111C could create a switch responsive to the reductive conditions of the microenvironment, potentially regulating its activity. Considering these previous observations, it is interesting to explore the shielding effect of a 16-polylysine peptide linked to the StIW111C membrane binding site via a disulfide bridge. Consequently, the reversibly bound polycation peptide could condition the mutant's pore-forming capacity to the presence of a reductive environment and concurrently its positive net charge would facilitate the binding to negatively charged molecules like nucleic acids.

Hence, the aim of this work was to study the ability of a conjugate based on the mutant StIW111C and a 16-polylysine peptide to biorespond to a reducing environment and promote the endosomal membrane permeabilization when it is associated to a model pDNA in order to improve its expression. Positive nanometric complexes were obtained by mixing pDNA with the conjugate and a cysteine-free polylysine peptide which served as a compacting agent (Fig. 1). However, the heterogeneity of these ternary polyplexes in size was higher compared with samples obtained from the binary mixture of pDNA and peptide. In vitro assays demonstrated the ability of the ternary polyplexes to permeabilize endosomes, but this was not the case of the binary complexes, although reporter gene expression was not observed with neither of these two nanoparticles. Albeit we have not a complete explanation for these findings, they could suggest that an insufficient proportion of the reducible conjugate is internalized into the endosomal compartment, most likely due to its entrapment within the smaller subset of large aggregates as observed through Cryogenic transmission electron microscopy (CryoTEM) imaging. Despite encountered challenges, the reducibility of the conjugate, along with its ability to associate with the nanometric complexes and permeabilize endosomes, underscore its potential as a component of non-viral vectors to enhance endosomal escape with further optimization.

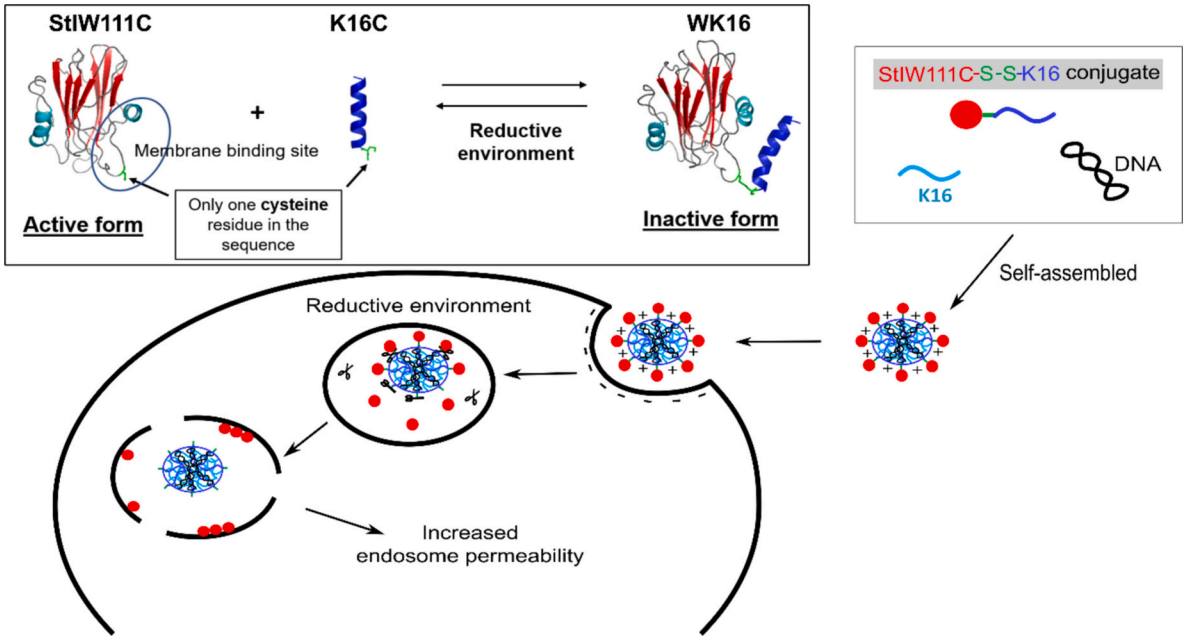

Fig. 1. Schematic representation of the proposed mechanism by which the reducible StIW111C-Polylysine conjugate may enhance endosomal permeability. The binding of K16C to StIW111C potentially blocks the membrane-binding site of StIW111C, resulting in a reversible inactive conjugate. This positively charged peptide K16, in combination with the conjugate, is hypothesized to form nanometric complexes with pDNA, facilitating cellular uptake. Once internalized, reductive conditions within the endosome may trigger the cleavage of the disulfide bridge. This reduction activates the StIW111C mutant, enabling it to bind irreversibly to the endosomal membrane disrupting the structural integrity of the endosomal compartment and lead to the release of pDNA into the cytoplasm.

2. Materials and methods

2.1. Materials

The plasmid tdTomato-C1 (5442 bp) was a gift from Michael Davidson (Addgene plasmid #54653; https://www.addgene.org/54653/; RRID: Adgene_54,653). The plasmid was acquired from *Escherichia coli* DH5 alpha bacteria, which had undergone transformation, and was cultivated on an agar culture medium. Subsequent isolation of the plasmid was performed utilizing the MaxiKit purification package (Qiagen, USA). DNA concentration was quantified through spectrophotometric analysis at both 260 and 280 nm wavelengths using the NanoDrop 2000c instrument (Thermo Fisher Scientific Inc., Wilmington, USA). Plasmid's integrity and purity were assessed via native DNA electrophoresis in a 1 % agarose gel. Linear PEI with a molecular weight of 25 KDa was sourced from Polysciences Inc. (Warrington, PA, USA). The remaining chemical reagents and materials were acquired from Sigma-Aldrich (St. Lois, MO, USA), unless is otherwise indicated.

2.2. Methods

2.2.1. Expression and purification of StIW111C

StIW111C expression was carried out in *Escherichia coli* Bl21 (DE3) PLYS strain, transformed with the PUC19 plasmid containing the StIW111C sequence. The protein was obtained by the self-induction approach [23], and recovered from the supernatants of the bacterial cell lysates employing as cationic exchanger a SP-Sepharose matrix (Cytiva, Massachusetts, USA) [24]. An additional washing step employing 100 mM β-mercaptoethanol (BM) was included prior to gradient elution for releasing molecules bound to the protein via cysteine residues [25]. The homogeneity of the purified protein was confirmed using 15 % PAGE-PAGE according to Laemmli [26]. The results are summarized in the supplementary Fig. S2. For protein labeling, 0.1 mg of protein was labeled with FITC (0.1 mg/mL in DMSO) in 1 mL of 500 mM carbonate buffer (pH 9.5) at molar protein/FITC ratio of 1–2. After 1-h incubation in the dark, the mixture was purified using a PD10 column.

2.2.2. Peptide synthesis

The synthesis of both the K16C and K16 peptides (with the C-terminals amidated) was carried out by the Center of Genetic Engineering and Biotechnology in Havana, Cuba, following standard Fmoc solid-phase methodologies and utilizing MBHA resin (substitution of 0.54 mmol/g) as the solid support with Fmoc-AM-OH as the spacer. Subsequent purification was carried out through reverse-phase high-performance liquid chromatography (RP-HPLC) (Shimatzu, Kyoto, Japan) to achieve a purity exceeding 95 %. The molecular masses of these peptides were determined via mass spectrometry. ESI-MS spectra were obtained using Q-T of 2 orthogonal hybrid configuration spectrometers (Micromass, England) with nanospray ionization source, resulting in an average molecular mass of 2170.96 and 2067.81 for K16C and K16, respectively.

2.2.3. StIW111C and K16C conjugation reaction

The peptide K16C was resuspended in 40 μL of acetate buffer at pH 5.0 and diluted to a final concentration of 2.5 mg/mL with 360 μL of the following buffer: 10 mM Na2HPO4/NaH2PO4, 1 mM EDTA, 30 mM NaCl, pH 6.7, previously equilibrated with N2 (g) for 30 min at 4 °C. StIW111C was treated with 100 mM BM for 15 min at room temperature to disrupt its potential homodimers. β-Mercaptoethanol was further removed using a pre-equilibrated molecular exclusion chromatography column (NAP10, Cytiva, Marlborough, MA, USA) in 0.1 M phosphate, 1 mM EDTA buffer at pH 8.0. This removal was timed to coincide with the drop-wise addition of the protein to the K16C peptide solution upon elution from the column in order to achieve a 1:10 StIW111C:K16C molar ratio. Dimethyl sulfoxide (DMSO) was added to the reaction mixture at a final concentration of 10 % or 20 % to promote an oxidative environment. The conjugation reaction was allowed to proceed at room temperature with agitation (800 rpm) on a KS 130 basic shaker (IKA, Staufen, Germany). The samples were centrifuged at 12,000*g* for 10 min and DMSO was removed from supernatant by filtration using 10 kDa Amicon Ultra-0.5 centrifugal filter unit. Both the supernatant and sediment were analyzed by native electrophoresis as described by Penton (2001) [21]. Briefly, Native-PAGE was conducted using a discontinuous system. Stacking gels composed of 5 % polyacrylamide polymerized in 143 mM HEPES–NaOH at pH 8.03 were employed, while resolving gels consisted of 12.5 % polyacrylamide polymerized in 375 mM HEPES–NaOH at pH 6.53. The running buffer used had a composition of 42 mM HEPES and 73 mM histidine at pH 7.0. Samples were dissolved in 112 mM Tris-HAc buffer containing 0.002 % methylene blue at pH 8.0. Subsequently, the Coomassie brilliant blue staining protocol by Studier (2005) was followed [23].

The analysis of conjugation efficiency over time involved the periodic extraction of aliquots from the reaction mixture. After eliminating DMSO from the supernatant, the reaction was halted by introducing iodoacetamide in a molar equivalent to the sulfhydryl groups present in the reaction. These aliquots were then subjected to analysis using the electrophoretic method describe by Penton (2001) [21]. Conjugation yield was quantitatively assessed through digital densitometry using ImageJ 1.54f (National Institute of Health, Bethesda, MD, USA).

2.2.4. Purification of the StIW111C-CK16 conjugate via cation exchange chromatography

The purification of the StIW111C-K16C conjugate, hereinafter referred to as WK16, was carried out via cation exchange chromatography using a 1-mL HiTrap CM Sepharose FF column (0.7 × 2.5 cm) (Cytiva, Marlborough, MA, USA) and an Äkta Go purification system (Cytiva, Marlborough, MA, USA). To achieve this, a low ionic strength buffer (0.02 M sodium phosphate at pH 6.7) and a high ionic strength buffer (0.02 M sodium phosphate with 1 M NaCl at pH 6.7) were employed. Elution was performed using a linear gradient of 0–1 M NaCl in the sodium phosphate buffer, with a total elution volume of 24 mL at 155.9 cm/h linear flow. The concentration of the purified conjugate was determined by measuring the absorbance at 280 nm of the fractions collected from the chromatogram peak, employing a NanoDrop 2000c spectrophotometer (Thermo Fisher Scientific, Waltham, MA, USA). The homogeneity of the conjugate was confirmed using native electrophoresis for basic proteins, following the protocol outlined by Penton et al. (2011) [21]. A total of 7 μg of polypeptide was loaded into each lane. Gels were stained using Coomassie brilliant blue dye.

2.2.5. Hemolytic activity of StIW111C-CK16 conjugate

The hemolytic assay experimental protocol received ethical approval from the Institute of Foods and Pharmacy's ethics committee, acting as the Institutional Review Board for the University of Havana. To prepare the erythrocyte suspension, fresh human blood collected from a minimum of five donors was mixed with sodium heparin (10–15 units/mL of blood). A standardized erythrocyte suspension was prepared by suspending erythrocytes in 10 mM Tris-HCl buffer pH 7.4, containing 145 mM NaCl [22]. Hemolytic activity was determined by following the reduction in turbidity of the erythrocyte suspension at 630 nm, utilizing a MULTISKAN EX microplate reader (Labsystems, Helsinki, Finland) as described [27]. The protein concentration ranged from 0.7 to 1440 ng/mL. Each sample was performed in triplicate at a controlled temperature of 25 ± 2 °C, preceded by a 15-min incubation period at ambient temperature without or with the presence of 100 mM β-Mercaptoethanol to disrupt disulfide bridges. Non-conjugated StIW111C treated with 100 mM β-Mercaptoethanol was used as a control in the hemolysis assay. Hemolysis after 15 min at each concentration was calculated using the following formula:

$$\%HA = \frac{A_0 - A_{(f)}}{A_0 - A_{max}} \times 100 \quad (1)$$

The calculation of hemolysis percentage (%HA) was derived from the observed absorbance values at 630 nm: A_o for the untreated erythrocyte suspension, $A_{(f)}$ for the suspension subjected to incubation with the free or conjugated forms of StIW111C, and A_{max} for the suspension incubated with an excess of StIW111C (0.02 mg/mL) following a 15-min period [22]. A graphical representation was constructed to illustrate the %HA as a function of protein concentration. The HC50 value which stands for the protein concentration necessary to achieve 50 % hemolysis, was determined by fitting the dataset to a Hill1 sigmoidal function using Origin Pro 8 software SR0 v80724 (Origin Lab Corporation, Northampton, MA, USA).

2.2.6. Preparation of DNA plasmid complexes

To prepare DNA complexes, the td-Tomato-C1 plasmid was mixed with an equal volume of either purified WK16 or the reaction mixture of polypeptides comprising WK16 and K16C, resulting in a final pDNA concentration of 20 μg/mL. All samples were diluted in nuclease-free water. The pDNA solution was gently added to WK16 while moving the pipette tip in a circular motion during the process. Subsequently, the mixtures were incubated at room temperature for 30 min before further utilization. The required amounts of WK16 to attain specific nitrogen/phosphorus ratios (R(N/P)), serving as a theoretical indicator of the positive-to-negative charge balance in the complex formation [28], were determined as follow.

$$n(2) = \frac{R(N/P) \times m(DNA)}{Mb \times \{[(1 - X2)/X2] \times q_0 1 + q_0 2\}} \quad (2)$$

The variable q_0i represents the number of basic groups per each polypeptide, with 17 corresponding to K16 (polypeptide 1), and 36 corresponding to WK16 (polypeptide 2), while n(i) represents the substance quantity of polypeptide *i*. X2 is the molar fraction of the conjugate WK16 in the mix of polypeptides. m(DNA) is the mass of DNA in the solution and Mb is the average molecular mass of a base (330 Da [29]). The mathematical procedure for deriving the formula is outlined in the supplementary information (Section 1).

2.2.7. Electrophoretic mobility-shift assay

DNA complexes were prepared following the previously described method (Section 2.2.6), utilizing 0.5 μg of td-Tomato-C1 and varying R (N/P) values from 0.5 to 5 using WK16. As a comparative control, free pDNA was included in the experimental setup. Additionally, an aliquot of the complex formed at the R(N/P) of 5 was subjected to a 15-min incubation with 5 units (Howell unit) of sodium heparin just before electrophoresis. These samples were applied onto a 1 % agarose gel submerged in TAE buffer (40 mM Tris, 20 mM Acetate and 1 mM EDTA pH 8.6) supplemented with 5 μg/mL of ethidium bromide. Electrophoresis was conducted at 100 V for 40 min. DNA bands were visualized using a UV light transilluminator EBOX VX5/20LM (Vilber Lourmat, France).

2.2.8. Cryogenic transmission electron microscopy

CryoTEM was used to assess DNA complexes formed from a mixture of WK16 and K16 (WK16-K-DNA), alongside those consisting solely of the K16 polypeptide (K-DNA) as control. These complexes were prepared at an R(N/P) of 10, as outlined in the Section 2.2.6, with the conjugate WK16 comprising 1 mol% of the polypeptide mixture by moles. This R(N/P) has been shown to be effective for transfection in various cell lines [30]. Prior to complex preparation, the conjugate was passed through a 0.22 μm filter (Sartorius, Göttingen, Germany). Complexes were generated in water for 30 min at room temperature. Imaging was performed using a JEOL JEM 2011 transmission electron microscope (JEOL, Tokyo, Japan) operating at 200 kV. Samples were placed on a perforated carbon grid or a copper grid coated with a perforated polymer film before being flash-frozen in liquid ethane. A Gatan 626 holder was used, and images were acquired using a Gatan RIO 16 camera using Digital Micrograph 3.50.3584.0 (Gatan Inc., Pleasanton, CA, USA). The analysis included quantifying the ratio of particles with maximum lengths above or below a 200 nm threshold, as well as assessing area and shape descriptors encompassing circularity, aspect ratio, and solidity. These measurements were performed using ImageJ 1.54f software (National Institute of Health, Bethesda, MD, USA).

2.2.9. Dynamic light scattering and zeta-potential measurement

Complexes containing WK16 were formed with a total R(N/P) ratio of 10, where the conjugate comprised 1 mol% of the polypeptide mixture by moles. In parallel, complexes generated with only K16 peptide were also prepared at the same R(N/P) ratio using the previously described methodology. The final DNA concentration was set at 20 μg/mL for size determination and 40 μg/mL for zeta potential assessment employing the Delsa Nano C instrument (Beckman Coulter, Brea, CA, USA). Statistical differences were evaluated through one-tailed Mann-Whitney analysis, facilitated by GraphPad Prism 9.5.1 software (GraphPad, San Diego, CA, USA).

2.2.10. Cell culture

HEK293T were routinely cultured in DMEMD-F12 supplemented with 10 % fetal bovine serum, 1 % streptomycin/penicillin, 2 mM glutamine (hereafter referred as completed medium) at 37 °C and 5 % CO_2. The cells were expanded at a ratio of 1:3 every three days. The confluence remained between 70 and 90 %. The cultures were maintained until the number of passages reach 15, after which they were discarded and a fresh cell culture was prepared.

2.2.11. Assessment of cell viability through MTT assay

The assessment of the complexes' cytotoxicity was conducted using the MTT assay. HEK293T cells were initially seeded at a density of 15,000 cells per well in 96-well plates and allowed to attain a confluence level ranging from 50 % to 80 % over an overnight incubation. Subsequently, the culture medium was substituted with 0.1 mL of fresh serum-free DMEM-F12. Complexes equivalent to 0.1 μg DNA were prepared with varying proportions of WK16 in the polypeptide mixture, ranging from 0 % to 4 %, resulting in final WK16 concentrations spanning from 0 to 1.4 μg/mL. After a 4-h incubation, 100 μL of fresh medium, supplemented with 20 % serum, was added, prolonging the incubation for another 24 h. The medium was then removed, and 200 μL of complete medium supplemented with 0.5 mg/mL of MTT was introduced, followed by a 2-h incubation period. The resulting formazan product, indicative of viable cells, was quantified spectrophotometrically at 570/650 nm using a TECAN infinite M200 PRO microplate reader (TECAN, Männedorf, ZH, Switzerland). The percentage of cell viability was determined relative to untreated control cells.

2.2.12. Cellular uptake experiments

The td-Tomato-C1 plasmid was fluorescently labeled with Cyanine 5 (Cy5) using the Label IT® Nucleic Acid Labeling Kit (Mirus Bio LLC, WI, USA). A total of 200,000 cells were seeded onto #1 coverslips (22 mm × 22 mm) designated for each treatment, or 70,000 cells in a 24-well plate, 24 h before treatments. The cells were exposed to DNA complexes formed at an N/P ratio of 10, employing either the polypeptide mixture comprising WK16 and K16 or the K16 peptide alone, and incubated for 4 h. For microscopic examination, following two washes with PBS containing 0.001 % sodium dodecyl sulfate (SDS) to remove surface-bound complexes [31], the cells were fixed in 4 % paraformaldehyde in PBS for 20 min at room temperature. Fixed cells underwent two additional PBS washes before nuclear staining with Hoechst 33342 at a concentration of 2 μg/mL for 15 min at room temperature. This was followed by two more washes with PBS. Subsequently, the cytoskeleton was labeled using Alexa Fluor™ 555 Phalloidin in accordance with the manufacturer's instructions (Thermo Fisher Scientific, MA, USA). After

another PBS wash, the transfected cells were visualized and examined using the Zeiss LSM 710 confocal microscope (Zeiss Group, Baden-Württemberg, Germany), equipped with an EC Plan-Neofluar 10×/0.30 objective lens. The respective fluorophores were excited at wavelengths of 355 nm (for the Hoechst 33342-nucleus), 543 nm (for the Alexa Fluor 546-cytoskeleton), 633 nm (for Cy5-pDNA) and 488 nm (for FITC-WK16). The co-localization between DNA and WK16 conjugate was quantified using the thresholded Mander's Colocalization Coefficient via the ImageJ plugin JACoP [32].

For flow cytometry analysis, cells were collected following the 4-h incubation period, washed twice with PBS containing 0.001 % SDS, and subsequently fixed in 2 % paraformaldehyde for 10 min at 4 °C. Uptake was assessed using the BD LSRFortessa™ Cell Analyzer (BD Biosciences, Franklin Lakes, NJ, USA).

2.2.13. Reporter gene expression analysis

For the transfection study, 70,000 cells were seeded per well in 24-well plates 24 h prior to commencing the transfection assay. Subsequently, the cells underwent treatment with pDNA complexes formed at an N/P ratio of 10, using either the polypeptide mixture comprising WK16 and K16 or K16 peptide alone, for a 4-h duration. Following this treatment, the solutions were removed, and the cells were cultured in 1 mL of complete growth medium for 48 h. The evaluation of tdTomato reporter gene expression was performed using flow cytometry employing the BD LSRFortessa™ Cell Analyzer (BD Biosciences, Franklin Lakes, NJ, USA). PEI was used as a positive transfection control under similar experimental conditions.

2.2.14. Evaluation of endosomal permeability change

An initial population of 200,000 HEK293T cells was cultured on #1 coverslips measuring 18 mm × 18 mm and incubated in complete medium supplemented with 1 mM calcein for 30 min. Following a triple wash with phosphate-buffered saline (PBS), the cells were exposed to serum-free DMEM-F12 containing unlabeled pDNA complexes either with the polypeptide mixture comprising WK16 and K16 or the K16 peptide alone for a 3-h incubation period, after which the treatment was removed. One set of cells was fixed with 4 % paraformaldehyde immediately after the 3-h incubation and subsequently analyzed using the Zeiss LSM 710 confocal microscope (Zeiss Group, Baden-Württemberg, Germany), equipped with an EC Plan-Neofluar 10×/0.30 objective lens. Another set of cells was maintained for an additional 24 h before fixation, and subsequent analysis was conducted using confocal microscopy.

2.2.15. Statistical analysis

Statistical analysis was performed using GraphPad Prism 9.5.1 software (GraphPad, San Diego, CA, USA). Statistically significant differences were analyzed by using two-tailed Mann-Whitney (for comparison of two groups) or Kruskal Wallis test with post-hoc Dunn's test (for comparison of more than two groups). A p value <0.05 was considered statistically significant ($^{*}p < 0.05$, $^{**}p < 0.01$, $^{***}p < 0.001$, $^{****}p < 0.0001$, absence of symbols, not significant).

3. Results

3.1. High yields of StIW111C-CK16 conjugate were attained in the conjugation reaction using DMSO

Bioinformatics modeling suggested that a 16-mer peptide should suffice to obstruct the membrane-binding site of StIW111C (data not shown). This computational insight led to experimental exploration of the conjugation of StIW111C and the K16C peptide under varied conditions, including both with and without DMSO. A molar ratio with StIW111C to K16C at 1:10 was selected to enhance effective heterotypic interactions between StIW111C and the peptide, while minimizing the possibility of homotypic interactions involving the mutant. The reaction between StIW111C and K16 results in the formation of the conjugate WK16, characterized by an intermediate electrophoretic migration position between the K16C peptide and StIW111C in a native electrophoresis (Fig. 2A, lane 3). When the reaction mixture is incubated with BM, the band representing this conjugate disappears, leaving only the bands of the two components visible (Fig. 2A, lane 4), strongly indicating that its formation involves a disulfide bridge. This finding effectively rules out the possibility of its formation through aggregation of the molecular species present.

Inclusion of DMSO in the reaction medium creates an oxidizing environment that promotes the formation of disulfide bonds facilitating the covalent and reversible binding of molecules [33,34]. Accordingly, the presence of DMSO in the reaction mixture significantly enhanced the conjugation yield of StIW111C and K16. Thus, 10 % DMSO in the reaction formulation increased yields from 50 % to values ranging between 80 and 90 %. This remarkable improvement in performance can be attained after a 7-h reaction period (Fig. 2B). Increasing the DMSO concentration to 20 % resulted in the formation of a precipitate containing the conjugate WK16, leading to a reduced yield that plateaued at only 50 % (Fig. S1). Consequently, it was decided to maintain the DMSO concentration at 10 % in subsequent conjugation reactions.

Next step involved the WK16 purification from the 10 % DMSO reaction mixture, which was conducted using a single-step cation exchange chromatography approach under similar conditions to those used for purifying the StIW111C mutant (Fig. S2). The chromatogram revealed two distinct absorbance peaks (Fig. 2C). The first peak corresponds to free StIW111C in the conjugation mixture, as evidenced by its elution within the conductivity range of 7.7–19.6 mS/cm (Fig. S2A and B). The second, displaying higher absorbance, corresponds to the conjugate of interest, which eluted at a conductivity of 69 mS/cm coinciding with the maximum absorbance value at 280 nm. The quantification of the area under the curve corresponding to these peaks of maximum absorption reaffirmed the attainment of a yield exceeding 80 % through the conjugation strategy used.

The purity of the conjugate was verified by a native gel electrophoresis for basic proteins [21] (Fig. 2D) which showed a single band corresponding to the pure conjugate in the absence of the reducing agent (lane 3). Upon incubation of the conjugate sample with BM (lane 4), this band with intermediate migration disappeared, leaving only the bands matching with the unconjugated variants of the mutant and the peptide (lanes 1 and 2, respectively).

Additionally, the mass spectra results for StIW111C and the purified WK16 conjugate, conducted to characterize and confirm conjugate formation, are presented in Supporting Information, Fig. S3. The experimental mass of StIW111C was determined to be 19,305.1 Da, closely matching the theoretical value of 19,307.74 Da and the reported by Valle et al (2018). The mass spectrum of the purified conjugate revealed an experimental molecular weight of 21,474.04 Da, consistent with its theoretical value.

3.2. Pore-forming activity of WK16 is activated in a reducing environment

Sticholysins are proteins known for their capacity to disrupt cytoplasmic membranes through pore formation [19,35]. A method commonly used in the functional characterization of these proteins and their mutants involves evaluating their hemolytic activity, which assesses their ability to lyse erythrocytes suspended in aqueous media. In this study, this assay was applied to determine the residual lytic activity of the purified conjugate in both the presence and absence of BM (Fig. 3).

In the absence of the reducing agent, the conjugate WK16 displayed negligible hemolytic activity under the experimental conditions. Nevertheless, the presence of 100 mM BM resulted in the restoration of hemolytic activity, albeit with an HC_{50} value that was 1.72 times lower compared to that of StIW111C employed as control under identical conditions.

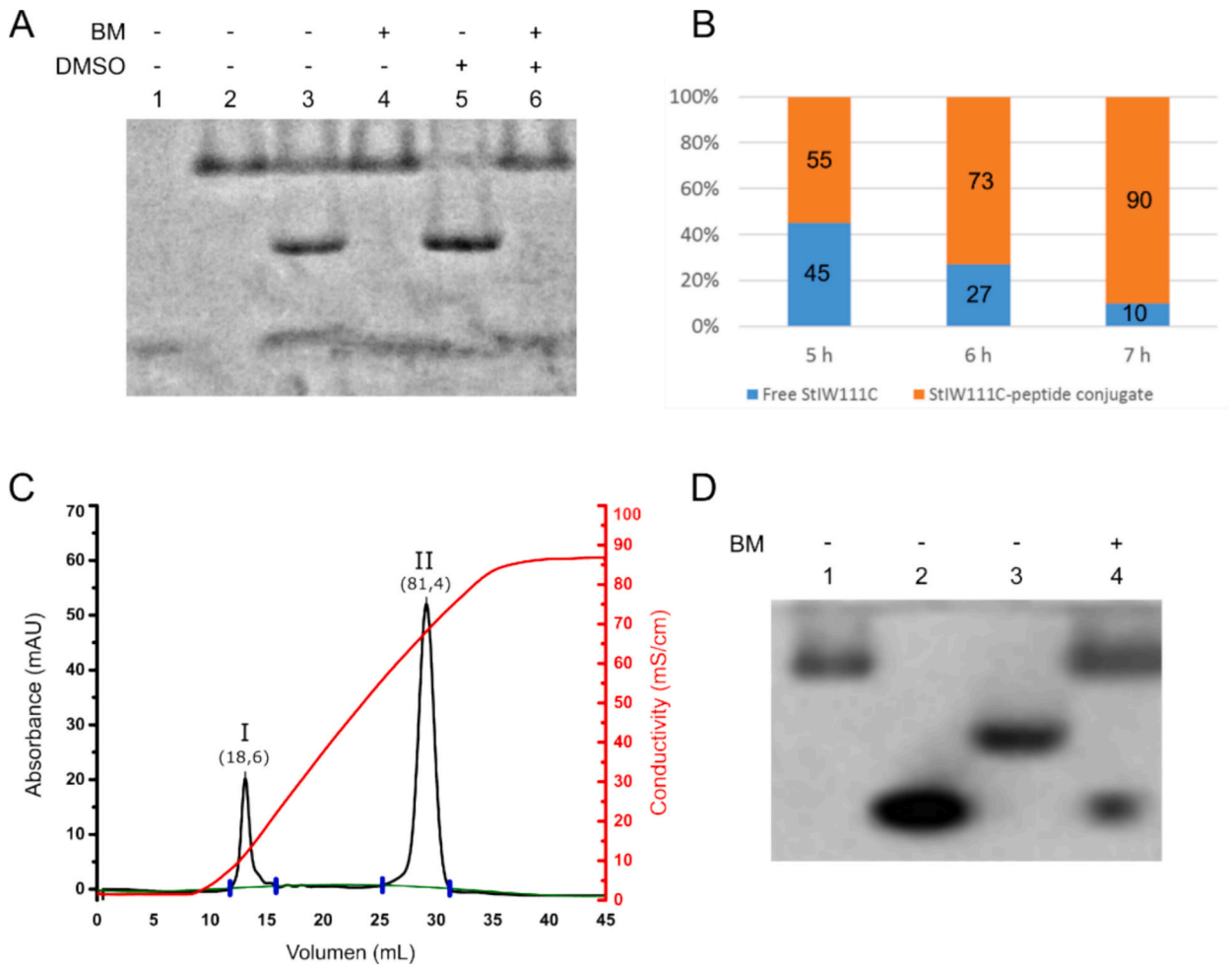

Fig. 2. StIW111C-CK16 conjugate production and purification. (A) Native gel electrophoresis of the resultant polypeptide mixture derived from the conjugation reaction, conducted with (+) or without (−) DMSO. Preceding additional treatments, the samples underwent DMSO removal through 10 kDa cutoff filtration. Control samples included 5 μg of K16C (lane 1) and StIW111C (lane 2). Reaction mixtures were subjected to incubation with (+) or without (−) BM for 15 min prior to electrophoresis (lanes 3–6), following the methodology outlined by [21]. (B) Evaluation of conjugation reaction yield attained in 10 % DMSO. At different time intervals during the conjugation reaction, an excess of iodoacetamide was added to reaction aliquots to hinder sulfhydryl group activity and avoid reoxidation. Subsequent to filtration, the conjugation reaction yield was estimated via densitometry analysis of the native electrophoresis gel. (C) Typical chromatographic profile of the conjugate WK16 purification by cationic exchange chromatography using 1 mL HiTrap CM-FF column. The graph depicts the variation in conductivity (red) and absorbance (black) during the elution of polypeptides under a linear ionic strength gradient. The absorption peaks are labeled as I and II. Percentages of areas under the curves delimited by vertical lines (blue) and the baseline (green) are indicated in parentheses. (D) Native electrophoresis for basic polypeptides. Samples were incubated for 15 min with or without BM prior to electrophoretic run at 120 mV. StIW111C protein (lane 1); K16 peptide (lane 2); purified conjugate, peak II (lanes 3–4).

3.3. Electrostatic-mediated formation of positively charged nanometric complexes between StIW111C-CK16 conjugate and pDNA

To assess the interaction capability of the purified conjugate with pDNA, samples containing 0.8 μg of the td-Tomato-C1 plasmid were incubated with varying amounts of the conjugate, achieving a range of N/P ratios from 0 to 5. The formation of DNA complexes at these specified R(N/P) was evaluated using the electrophoretic mobility shift assay (Fig. 4). Starting at R(N/P) of 1, complete disappearance of the band corresponding to free DNA was observed, concomitant with the appearance of a band near the point of application, which ceased to be observable at higher ratios. To ascertain whether the band disappearance resulted from the electrostatically mediated formation of complexes between WK16 and DNA, an aliquot of the sample generated at R (N/P) of 5 was incubated with sodium heparin. The addition of sodium heparin led to the restoration of the pDNA band's migration demonstrating that the vanishing of the band did not stem from pDNA degradation but rather from the formation of the WK16-pDNA complex, facilitated by electrostatic interactions.

In subsequent experiments aimed at the formation of DNA complexes, a 16-lysine peptide devoid of cysteine at its C-terminal end (K16) was used as the compaction agent [30]. Consequently, binary complexes were produced as controls, comprising exclusively of K16 and pDNA (K-DNA), and ternary complexes were generated including, in addition to the aforementioned components, the WK16 conjugate (WK16-K-DNA). In order to generate ternary DNA complexes involving PFPs, previous investigations have used proportions within the range of 0 to 0.6 mol% for the incorporation of the Listeriolysin O-Protamine fusion protein [8], or 1.0–3.5 % (*w*/w) of the Listeriolysin O-PEI disulfide-linked conjugate, which is equivalent to 0.4–1.5 mol% [7]. In consequence in the present work, we selected 1 mol% relative to the total polypeptidic substance present for the inclusion of the WK16 conjugate into the preparations.

The DNA complexes, formed in the presence or absence of WK16, were analyzed using CryoTEM (Fig. 5). Prior to complexes' preparation, the conjugate was filtered through a membrane with an average pore size of 0.22 μm to eliminate potential large aggregates. The reduction in conjugate concentration due to filtration was found to be <10 %.

In the micrograph, the presence of the conjugate in the DNA complex

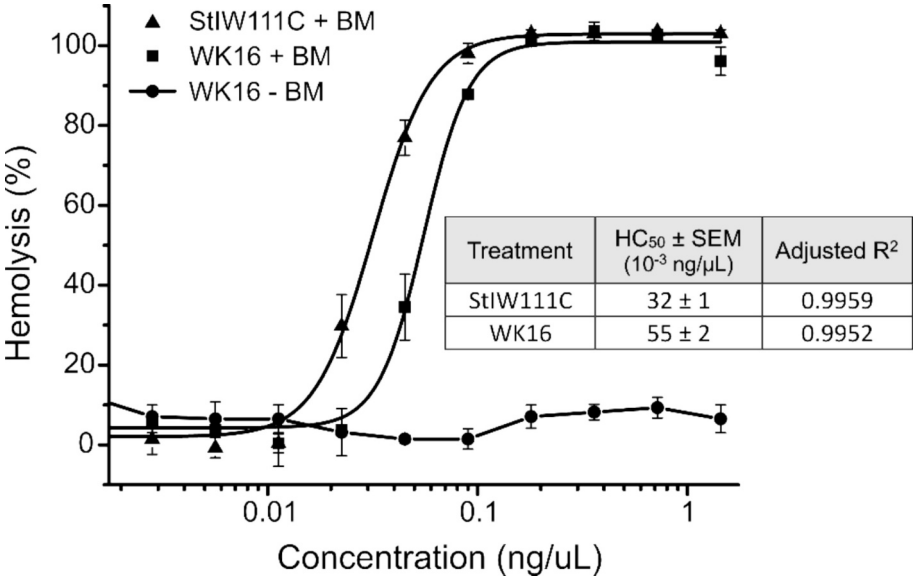

Fig. 3. Hemolytic activity of the purified StIW111C-CK16 conjugate. The graph depicts the fitting of Hill's sigmoidal curve to hemolysis data obtained at varying concentrations of the purified conjugate in the presence (■) or absence (●) of BM. Additionally, the lytic activity of the StIW111C mutant was assessed in the presence of the reducing agent (▲). (Inset) The protein concentration at which 50 % hemolysis is achieved for the distinct treatments is determined through fitting to Hill1 sigmoidal function (HC_{50} ± SEM; SEM: standard error of the mean).

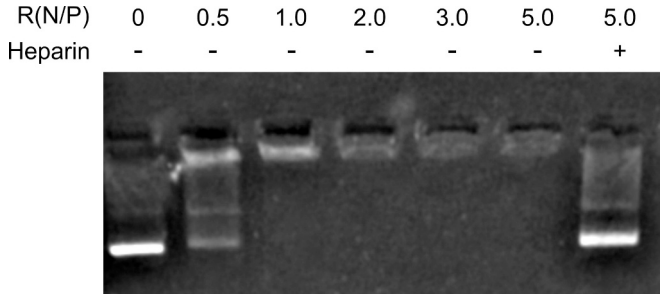

Fig. 4. Assessment of the Interaction between StIW111C-CK16 conjugate and pDNA through EMSA. Complexes were generated by incubating different quantities of WK16 with pDNA for 30 min. The pDNA concentration in each sample was adjusted to 20 μg/mL. These complexes were loaded onto a 1 % agarose gel at a uniform equivalence of 0.8 μg of DNA per lane. The upper portion of the figure displays the R(N/P) employed indicating which samples were subjected to incubation with (+) or without (−) sodium heparin for 15 min immediately following complex formation.

assembly induced aggregate formation (indicated by black arrows), in contrast to the preparation lacking the conjugate (Fig. 5A). The latter was primarily characterized by the emergence of nanoscale structures (highlighted by white arrows). To assess whether aggregates prevailed over nanoscale structures in the samples of the ternary complex formation, particles with a maximum length (L) equal to or exceeding 200 nm were quantified separately from those measuring <200 nm. It was observed that while aggregates (particles larger than 200 nm) were present, complexes smaller than 200 nm constituted the predominant population within the sample (Fig. 5B, upper panel).

The association of WK16 with complexes with a maximum length below 200 nm was further validated by conducting a comparative analysis of the size (area) between WK16-K-DNA complexes and K-DNA complexes (Fig. 5B, lower panel). This analysis unveiled a notably greater area for DNA complexes generated in the presence of WK16, strongly indicating the association of the WK16 protein into these complexes. The nanometric complexes observed in both DNA complex formulations exhibiting toroidal configurations, as confirmed by modification in the inner gray values, as well as spherical and rod-like morphologies (Fig. 5C, upper panel). However, in both sample sets, predominant nanocomplexes displayed smooth rod-like configurations, as evidenced by shape descriptors previously referenced [36,37], with mean values for circularity, aspect ratio, and solidity approximately 0.7, 2.0, and 0.9, respectively (Fig. 5C, lower panel).

Dynamic light scattering technique (DLS) was employed to characterize the same samples previously examined via CryoTEM. This method enables the correlation of particle diffusion in a diluted medium with the dimensions of a rigid sphere, facilitating the estimation of the relative dimensions of the particle system based on its diffusion coefficient [38]. In Fig. 6, a noticeable rightward shift and an increase in the amplitude of the intensity-based size distribution curve were observed for the WK16-K-DNA complexes compared to K-DNA. The mean hydrodynamic diameter of the particles increased from 80.4 ± 1.4 nm for K-DNA to 125.0 ± 0.8 nm for the WK16-K-DNA complexes, accompanied by a 1.55-fold increase in the polydispersity index from 0.209 ± 0.021 to 0.324 ± 0.015, respectively (Fig. 6). The *Z*-potential values were determined for both complexes, demonstrating a similar positive charge for both: +17.0 ± 1.7 mV (K-DNA) and + 18.2 ± 2.1 mV (WK16-K-DNA). These characteristics observed by DLS are commonly replicated across various conjugate batches derived from distinct conjugation reactions.

3.4. Permeabilization of the endosomal compartment by DNA complexes containing StIW111C-CK16 conjugate

Once the feasibility of forming WK16-K-DNA ternary complexes on the nanoscale and with a positive charge was established, an assay was conducted to assess the impact of incubating these particles on the viability of the highly transfectable HEK293T cell line. The cells were incubated for 24 h with particles generated at an R(N/P) of 10 using different proportions of WK16. The amount of DNA added to each treatment was 0.1 μg. Substantial loss of cell viability occurred only when the conjugate proportion within the complexes exceeded 2 % in the formulation (Fig. 7A).

The uptake of the K-DNA and WK16-K-DNA complexes, assembled at an R(N/P) of 10 with a 1 mol% proportion of the WK16 conjugate in the polypeptide mixture, was assessed in the HEK293T cell line after a 4-h incubation period. Using confocal microscopy (Fig. 7B), substantial

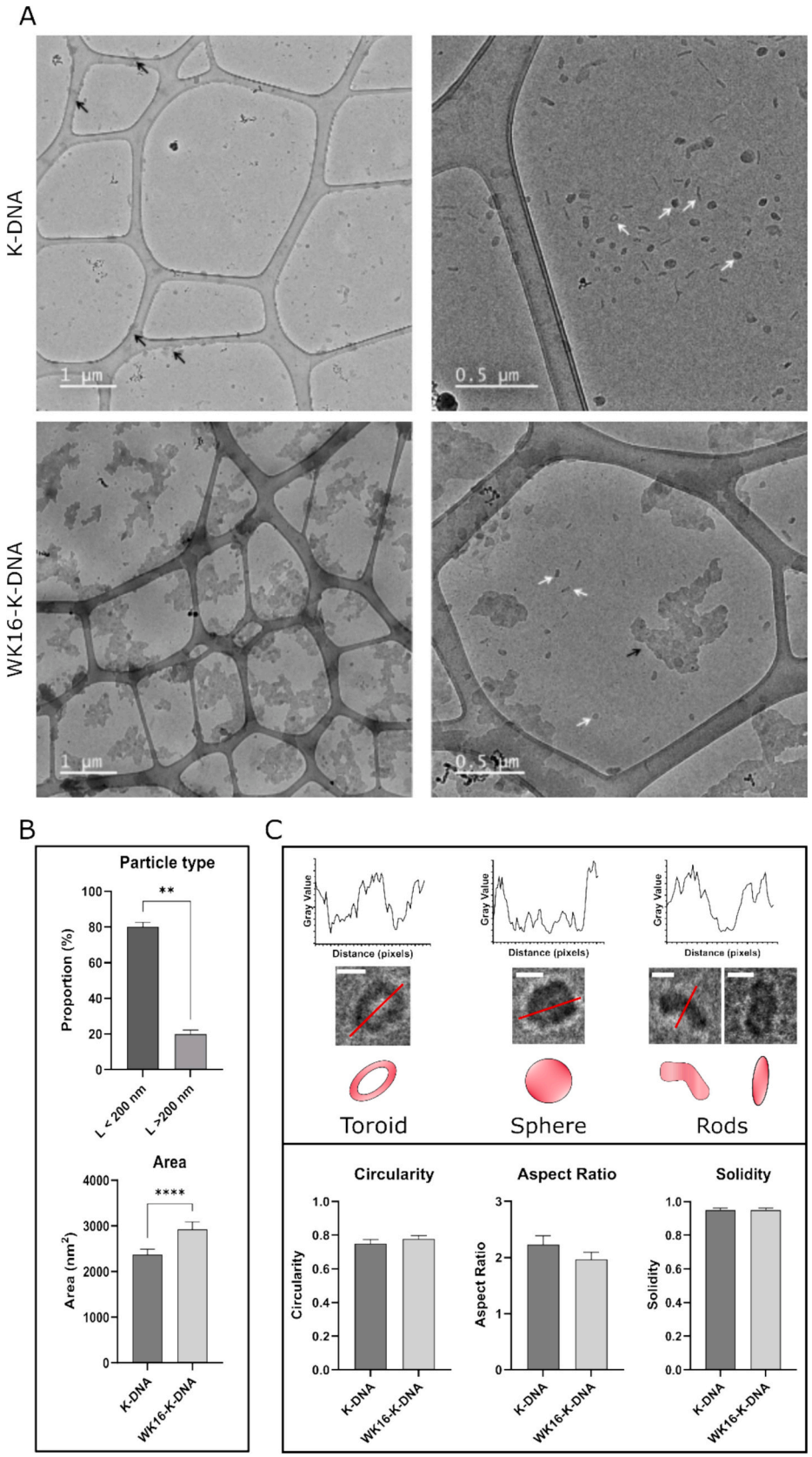

(caption on next page)

Fig. 5. Cryo-transmission electron microscopy of the K-DNA and WK16-K-DNA complexes. K-DNA and WK16-K-DNA complexes were formed by incubating their components for 30 min at room temperature in nuclease-free water. (A) Flash-frozen samples were subjected to transmission electron microscopy. The white line in the images represents the scale used. White arrows indicate representations of complexes with the largest length <200 nm, while black arrows indicate the presence of aggregates. (B) The upper graph depicts the proportion of particles with the maximum length either below or above 200 nm within the WK16-K-DNA ternary complex sample ($n = 200$). The area of particles with the largest length below 200 nm was calculated using ImageJ software and subsequently compared for both types of complexes in the lower graph ($n = 135$). (C) The upper panel displays the observed shapes for the K-DNA and WK16-K-DNA complexes samples with the largest length under 200 nm. Graphs exhibit grayscale values along the red line in representative microscopy images for each of these shapes. The 30 nm scale is denoted by a white line in the images, along with an accompanying outline of the observed forms. The lower panel presents the shape descriptors assessed for each preparation. Graphs show the mean ± SEM. Statistical significance, determined using Mann Whitney test, is indicated by $^{**}p < 0.01$ or $^{****}p < 0.0001$.

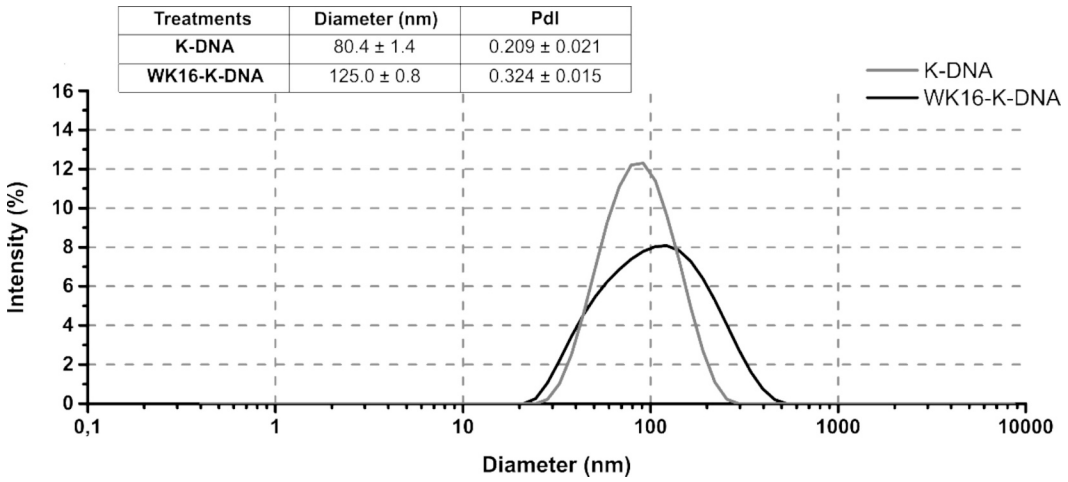

Fig. 6. DNA complexes containing StIW111C show larger sizes and polydispersity. An overlay of intensity distributions for K-DNA (Gray) and WK16-K-DNA (black) complexes is presented. The table shows the mean diameter and polydispersity index (PI) for each treatment. All assays were performed in triplicate and the mean ± standard deviation (SD) is reported.

levels of internalization of fluorescently labeled DNA were observed, with nearly all nuclei hosting at least one adjacent particle, a trend consistent across both K-DNA and WK16-K-DNA complexes. Three-dimensional confocal microscopy images of the cells offered visual confirmation of complex internalization, as the DNA signal within the complexes (red) was surrounded by the signal indicative of the cellular cytosol (magenta) (Fig. S4). Flow cytometric quantification following a 4-h exposure indicated that over 75 % of cells contained the complexes, with no significant differences between K-DNA and WK16-K-DNA treatments (Fig. 7C), mirroring the uptake levels observed with PEI-DNA treatment.

We quantified the co-localization between DNA (red channel) and the WK16 conjugate (green channel) using the Thresholded Mander's Colocalization Coefficient via the ImageJ plugin JACoP [32]. This coefficient measures the portion of overall probe fluorescence that overlaps with the fluorescence emitted by a second probe. We opted for this metric over the Pearson Coefficient due to its sensitivity primarily to co-occurrence, rather than signal proportionality [39]. Even though DNA and WK16 may co-occur within the same complexes, their presence in a fixed proportionality is not guaranteed across the sample. The average colocalization between the WK16 conjugate and DNA was 71.1 % across 360 cells, whereas only 19.8 % colocalization was observed between DNA and the protein.

Despite the heightened internalization levels of the DNA in complex with polypeptides, the expression of the tdTomato reporter gene was notably lower in comparison to the levels attained with the transfection agent PEI (Fig. 7D). The marked disparity between the limited expression levels of the reporter gene and the substantial internalization of DNA complexes within the HEK293T cell line prompts an intriguing question: Does the WK16 conjugate, present within the complex, undergo activation within the endosomal compartment? To elucidate this inquiry, the endosomal compartment was pre-loaded with the ionic fluorophore calcein, incapable of passing through the cell membrane. Subsequently, after removal of non-internalized fluorophore, cells were subjected to a 3-h incubation with the complexes. The release of this fluorophore to cell cytosol was analyzed using confocal microscopy at 3-h and 24-h time points following the initiation of the treatment (Fig. 8). After 3 h of incubation only the presence of endosomal compartments laden with the fluorophore was observed in both treatment groups. Nevertheless, at 24-h a solely diffused fluorescence pattern was discernible in WK16-K-DNA-treated cells, while only minor remnants of the fluorophore were detectable in K-DNA-treated cells.

4. Discussion

Effective gene therapy demands the development of gene transfer vectors that safeguard nucleic acids from degradation by nucleases, evade immune responses, extend in vivo circulation, and traverse physiological barriers [40,41]. While non-viral vectors such as cationic liposomes and polymers offer safety, versatility, and the potential for functionalization and tissue-specific targeting with minimal cytotoxicity, their clinical utility is hindered by hurdles that result in low transfection efficiency [42].

Enhancing the efficiency of non-viral delivery systems faces a critical challenge: their limited ability to escape the endosomal compartment upon cellular internalization [43]. Addressing this challenge requires the inclusion of elements that promote escape, thus ensuring the release of large macromolecular cargo. Some of these systems have employed pore-forming proteins, such as the bacterial LLO [8], to enhance cargo release.

StIW111C is a mutant derived from the pore-forming protein StI, with cysteine replacing tryptophan at position 111, a critical site in the protein's membrane interaction [21,22]. To make it suitable for gene delivery, controlling its nonspecific activity to adapt to its environment is essential. While the reducing conditions in the endosomal compartment are debated [44], several disulfide-based redox-sensitive strategies

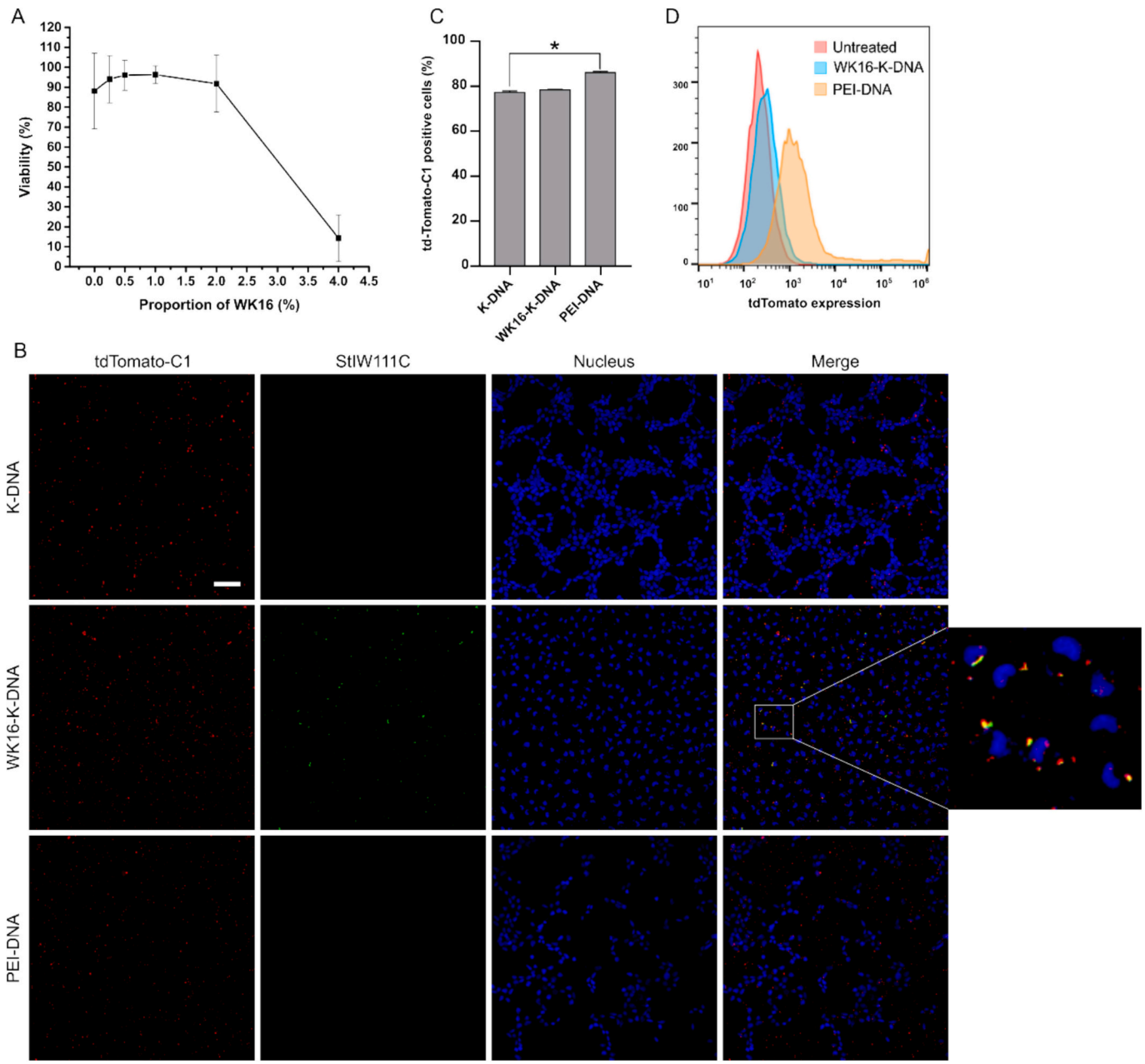

Fig. 7. Assessment of cell viability, pDNA complex uptake, and tdTomato reporter gene expression. (A) Cell viability in HEK293T cells was assessed via the MTT assay after treatment with DNA complexes. Cells were seeded at 15,000 cells per well in 96-well plates, exposed to DNA complexes with a constant R(N/P) ratio of 10 for 4 h, followed by removal of treatments and further culture for 24 h. The WK16 concentration within the complex varied from 0 % to 4 % of the polypeptide mixture, resulting in a final concentration of WK16 ranging from 0 to 1.4 ng/mL. (B) Internalization of complexes into HEK293T cells was examined using confocal microscopy. Cells were seeded at a density of 200,000 cells per well in 24-well plates and incubated with K-DNA, WK16-K-DNA and PEI-DNA complexes, equivalent to 1 μg of DNA at R(N/P) of 10, for 4 h in serum-free medium. Following incubation, cells were washed twice with PBS containing 0.001 % SDS to remove any remaining extracellular polyplexes. Fixed in 3.5 % paraformaldehyde, the cells were analyzed using confocal microscopy. The td-Tomato-C1 plasmid, WK16 conjugate, and cell nuclei were respectively stained with Cy5 fluorophore (red), FITC (green), and Hoechst 33342 (blue). (Scale bar: 20 μm). (C) 70,000 cells were seeded in 24-well plates and incubated with 0.3 μg of Cy5-labeled td-Tomato-C1 in similar experimental conditions as described in B. After incubation, cells were washed twice with PBS containing 0.001 % SDS, and the uptake was quantified using flow cytometry. Statistical significance, determined using Kruskal Wallis test with post-hoc Dunn's test, is indicated by * ($p < 0.05$). (D) Flow cytometry analysis was conducted to assess tdTomato expression. The expression of the fluorescent protein tdTomato was evaluated 48 h after treatment removal. As a positive transfection control, DNA complexes were formed using the polycation PEI at R(N/P) = 10.

have been used [45,46]. It's generally accepted that the endosomal compartment has lower reducing conditions compared to the cytosol, which could reduce the rate of disulfide bond cleavage and hence the timing of protein activation during endosomal maturation [44].

To modulate the activity of the StIW111C mutant in response to a reducing environment, it was linked to a 16-lysine basic peptide via a disulfide bridge. While polylysine peptides have been used in nucleic acid delivery systems, their transfection efficiency is reduced due to complex entrapment within the endosomal compartment [47]. Initially, a 20 % DMSO solution was used during the conjugation process. However, it led to precipitate formation in the reaction mixture, trapping a significant portion of the conjugate and peptide within it. While the protein recovered from the precipitate retained its hemolytic activity in its reduced state, separating the sediment added an extra step that could

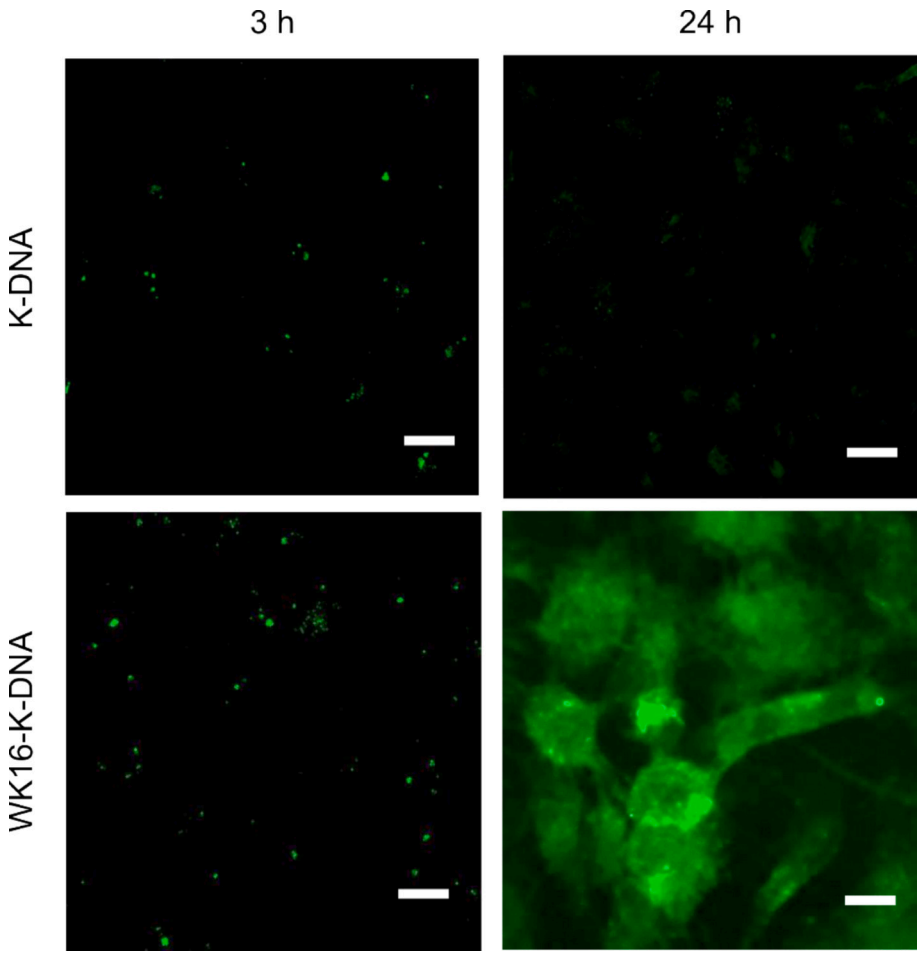

Fig. 8. Endosomal permeabilization in HEK293T cells mediated by WK16-K-DNA complexes. A population of 200,000 cells was seeded and subsequently treated with 1 mM calcein for 15 min. Following calcein exposure, the cells were rinsed four times with PBS prior to a 3-h treatment with K-DNA or WK16-K-DNA complexes. The treatment was then removed after the 3 h. One subgroup was promptly fixed with 3.5 % paraformaldehyde, while another subgroup was incubated for an additional 24 h before fixation. Both sample subgroups underwent analysis via confocal microscopy (scale bar: 20 μm).

impact conjugate yields. The relatively nonpolar nature of DMSO likely promoted intermolecular attractions among polypeptide chains, leading to aggregation. Arakawa et al. (2007) found that increasing DMSO concentrations altered protein interactions, favoring binding to DMSO over hydration, leading to self-association and precipitation [48]. Accordingly, reducing DMSO concentration to 10 % significantly improved conjugation yields (82 %) and disrupted the tendency for polypeptide aggregation.

The reversible inactivation of StIW111C in its conjugated form was demonstrated by a simple hemolytic assay. Under the assayed experimental conditions, the WK16 conjugate displayed complete inactivity in the absence of the redox environment provided by BM. However, in the presence of the reducing agent, its activity was restored, albeit with an HC_{50} parameter 1.7 times higher than that of unconjugated StIW111C used as a control (inset to Fig. 3). Remarkably, the recovery of activity in the reducing environment aligns with the separation of conjugate components observed in native electrophoresis (Fig. 2D). These results indicate that reversible binding of the peptide to the mutant inactivates StIW111C and that this protein undergoes certain modifications during conjugation, exhibiting a reduced activity. It has been well-established that DMSO can induce destabilization of protein secondary structures and promote methionine oxidation [33,49]. Nevertheless, the lower activity observed in the conjugate have limited implications for practical applications due to the inherently high activity of this protein [19,27,50].

Through the implementation of this regulatory mechanism, it may be feasible to achieve localized activation of the mutant, thereby preventing its binding with the outer monolayer of the cytoplasmic membrane. It is essential to emphasize that this strategy does not preclude the potential for the protein to remain functionally active within the reducing environment of the cytosol subsequent to facilitating the nucleic acid's endosomal escape. Sticholysins exhibit pore-forming activity that remains unaffected over a wide pH range [51]. Consequently, following protein activation within the endosomal environment, any potential inactivation of its functionality in response to pH changes upon transitioning to the cytosol, or via the formation of novel disulfide bonds, is unlikely. Nonetheless, StIW111C inactivation may occur through its binding to the endosomal membrane once reduced, depending on the amount of conjugate present in the DNA complex. Substantiating this notion, there exists evidence indicating the irreversibility of sticholysins binding to lipid membranes containing sphingomyelin. When human erythrocytes were exposed to the supernatant obtained from a combination of StII and liposomes containing sphingomyelin, a reduced lytic capacity was noted in comparison to the supernatants resulting from incubations with sphingomyelin-free liposomes [52]. It was concluded that the reduced activity stemmed from decreased StII concentration in the supernatant, caused by irreversible binding to the sphingomyelin-containing liposomes.

The electrophoretic mobility shift assay is used to establish whether an electrostatic interaction occurs between DNA and a polycation [53]. In the experiment carried out, all the DNA was part of the complex at R (N/P) of 1 (Fig. 4). Curiously, it is not possible to see the DNA band at

ratios equal to or >1. This could be due to the fact that a larger R(N/P) promotes a higher compaction of the DNA, preventing the intercalation of ethidium bromide between nucleotides [54]. The detection of the free DNA band in the sample where complex formation occurred at an R(N/P) of 5 after incubation with heparin, suggests that the absence of this band in the identical sample lacking this anionic competitor does not result from DNA degradation (Fig. 4). Furthermore, these results confirm that the DNA complex formed in the presence of the WK16 conjugate is established by electrostatic interaction and that it is reversible.

The dissociation of nucleic acid complexes represents an important parameter to be considered when designing an effective delivery system for nucleic acids. Upon arrival in the cytosol or cell nucleus, it is imperative for DNA to undergo dissociation from the complex to enable transcription and replication processes [40]. Within the cellular cytosol and nucleus, a multitude of negatively charged molecules, primarily phosphorylated moieties, may serve as electrostatic competitors, thereby facilitating the dissociation of these complexes.

When employed in transfection, the ternary WK16-K-DNA complexes exhibit a reduced propensity to support the expression of the reporter gene tdTomato, even in cases of extensive internalization and increased of endosomal permeability (Figs. 7 and 8, respectively). In order to explore a possible correlation between the physical characteristics of the complexes and their transfection efficiency, the complexes were analyzed through cryogenic electron microscopy (Fig. 5) and dynamic light scattering (Fig. 6). These analyses unveiled that the strategy employed to generate the WK16-K-DNA complexes results in the formation of aggregates within the formulation. However, these entities represent a minority in comparison to nanometric rod-like particles with the predominant length below 200 nm. DLS measurements further validate the prevalence of smaller particles in contrast to aggregates.

Analysis of the average dimensions of WK16-K-DNA complexes relative to K-DNA, as illustrated in Figs. 5B and 6, suggests the potential association of WK16 with the nanosized complexes. However, approximately 40 % of the WK16 conjugate is retained within the largest complexes and aggregates, as estimated by hemolytic activity following filtration of the WK16-K-DNA complexes through a 0.45 μm filter (result not shown). Visual examination of confocal images (Fig. 5B) alongside the Thresholded Mander's Colocalization Coefficients suggest that the DNA complexes generated in the presence of WK16 and internalized by HEK293T cells harbored the WK16 conjugate because it intracellularly colocalizes approximately in a 71 % with DNA. The low proportion of WK16 conjugate, comprising <1 mol% of the polypeptide mixture, may explain why only 19.8 % of the total DNA fluorescence colocalizes with the fluorescence of the WK16 conjugate.

Considering the Stokes radius of the StIW111C monomer and dimer is 2.97 nm and 4.45 nm, respectively [22], and using the maximum radius possible for the conjugate WK16 of 4.45 nm, its maximal cross-sectional area could be 62.2 nm^2. On the other hand, the average area of complexes ternary (WK16-K-DNA) is 2927.5 nm^2 (Fig. 5B), resulting about 47 times larger than the conjugate. Given that we can find as maximum in the complexes only 1 % WK16, it would be possible to depict the distribution of WK16 as dots in their surface justifying the high and low percentage of the protein or DNA, respectively, interacting between each other.

The presence of the largest complexes and aggregates, albeit in limited amount, may hinder the endosomolytic activity of the protein by reducing optimal internalization. This could result in an insufficient amount of protein reaching the endosomal compartment, thereby limiting pore formation and impairing the disruption of the endosomal membrane, which is essential for the release of nanocomplexes. Of note, the observed increased permeability of the endosomal membrane (Fig. 8) suggests the presence of pores. It is important to highlight, however, that the formation of even a single pore with a diameter as small as 2 nm, such as those induced by StI [35], would be adequate to permit the escape of small fluorophores like calcein from the endosome, but not the WK16-K-DNA nanocomplexes of average size around 100 nm. The calcein release assay showed endosomal release occurs within 3 to 24 h post-treatment. The redox potential in endosomes and the three-dimensional conformation of WK16 may hinder disulfide bond reduction, slowing endosomal permeabilization. Additionally, the insufficient accumulation of WK16 within the endosomes likely contributes to the slower kinetics of endosomal permeabilization. This slower process limits the conjugate-mediated escape of particles from endosomes before DNA degradation, which likely accounts for the observed low expression levels.

5. Conclusions

In conclusion, our study has shed light on the potential of the bio-responsive WK16 conjugate as a tool for enhancing the escape of nucleic acid complexes from endosomes. The design of this conjugate, which leverages the innate pore-forming capabilities of StIW111C while enabling controlled responses in reductive environments, holds promise for improving gene delivery in non-viral systems. However, our findings have also highlighted the critical need for refining the formulation, as the unexpected entrapment of the reducible conjugate within aggregates probably hindered the desired expression of a reporter gene. The heterogeneity observed within the ternary WK16-K-DNA complex formulations underscores the imperative for a redesign aimed at minimizing aggregate formation. Other limitations of the current design include the low proportion of WK16 conjugate that can be incorporated into the DNA complex formulation due to its observed cytotoxicity probably as consequence of the protein residual activity in the cell cytosol. Therefore, the new design should lead to inactivate the protein in the cytosol, allowing for a higher level of conjugate to be used in the formulation. Our research offers a starting point refining and optimizing the WK16-based complexes. Potential modifications include altering the condensing agent, incorporating signals for cytosolically inhibiting pore-forming activity and also nuclear localization signal sequences. These strategies aim to enhance endosomal escape and improve gene expression, thereby maximizing the therapeutic potential of the conjugate.

CRediT authorship contribution statement

Felipe A. Escalona-Rodriguez: Writing – original draft, Investigation, Formal analysis, Conceptualization. **Javier La O-Bonet:** Writing – review & editing, Investigation, Formal analysis. **Lidia Priscila Ferrer Tasies:** Writing – review & editing, Investigation. **Karthikeyan Subbarayan:** Writing – review & editing, Investigation. **Ada L. Rivero-Hernández:** Writing – review & editing, Investigation. **Maricary Sifontes-Niebla:** Writing – review & editing, Investigation. **Alexis Manso-Vargas:** Resources, Investigation. **Luisa De Cola:** Supervision, Resources. **Nora Ventosa:** Writing – review & editing, Supervision, Resources. **Belinda Sánchez:** Supervision, Resources. **Carlos Alvarez:** Writing – review & editing, Resources. **Daniel G. Rivera:** Writing – review & editing, Resources, Funding acquisition. **Barbara Seliger:** Writing – review & editing, Supervision, Resources. **María E. Lanio:** Writing – review & editing, Supervision, Project administration, Funding acquisition, Formal analysis, Conceptualization.

Declaration of generative AI and AI-assisted technologies in the writing process

During the preparation of this work the author(s) used ChatGTP3.5 in order to improve only readability and language. After using this tool/service, the author(s) reviewed and edited the content as needed and take(s) full responsibility for the content of the publication.

Funding

This work was supported by the European project Horizon 2020 NanoOligoMed (H2020-MSCA-RISE-2017, UE-778133); DAAD (Bonn, Germany) with funds from the German Federal Foreign Ministry (AA), (project ID 57592717, DAAD Health Center GLACIER); the Center of Molecular Immunology of Cuba; and National Program for Nanoscience and Nanotechnology (PN3) of the Ministry of Science, Technology and Environment of the Republic of Cuba (Project PN211LH008-017).

Declaration of competing interest

The authors declare that they have no known competing financial interests or personal relationships that could have appeared to influence the work reported in this paper.

Acknowledgement

The authors gratefully acknowledge the University of Strasbourg and Nanomol Technology SL for their generous provision of access to confocal microscopy and cryo-transmission electron microscopy, respectively. We extend our sincere appreciation to the Horizon 2020 projects, NanoOligoMed and GLACIER, for supporting FAER's research stays at the afore mentioned institutions and Martin Luther University Halle-Wittenberg. We also express our deep gratitude to Dr. Gregor Sachse of Brandenburg Medical School for his invaluable training in confocal microscopy, and to Dr. Hilda Garay of the Center for Genetic Engineering and Biotechnology in Havana, Cuba, for synthesizing the K16 peptide. Additionally, we thank Alena Soboleva and the Institute for Plant Biochemistry (Halle, Germany) for their support with mass spectrometry analysis.

Appendix A. Supplementary data

Supplementary data to this article can be found online at https://doi.org/10.1016/j.ijbiomac.2025.139819.

Data availability

Data will be made available on request.

References

[1] K.I. Cupic, J.J. Rennick, A.P. Johnston, G.K. Such, Controlling endosomal escape using nanoparticle composition: current progress and future perspectives, Nanomedicine (London, England) 14 (2) (2019) 215–223. Epub 2018/12/05. doi: 10.2217/nnm-2018-0326. PubMed PMID: 30511881.

[2] S. Chatterjee, E. Kon, P. Sharma, D. Peer, Endosomal escape: a bottleneck for LNP-mediated therapeutics. Proceedings of the National Academy of Sciences of the United States of America 121 (11) (2024) e2307800120. Epub 2024/03/04. doi: 10.1073/pnas.2307800120. PubMed PMID: 38437552; PubMed Central PMCID: PMCPMC10945858.

[3] C. Qiu, F. Xia, J. Zhang, Q. Shi, Y. Meng, C. Wang, et al., Advanced strategies for overcoming endosomal/lysosomal barrier in nanodrug delivery, Research (Washington, DC) 6 (2023), 0148. Epub 2023/05/30. doi: 10.34133/research.0148. PubMed PMID: 37250954; PubMed Central PMCID: PMCPMC10208951.

[4] J.G. Schellinger, J.A. Pahang, R.N. Johnson, D.S. Chu, D.L. Sellers, D.O. Maris, et al., Melittin-grafted HPMA-oligolysine based copolymers for gene delivery, Biomaterials 34 (9) (2013) 2318–2326. Epub 2012/12/25. doi: 10.1016/j.biomaterials.2012.09.072. PubMed PMID: 23261217; PubMed Central PMCID: PMCPMC3552146.

[5] D.J. Peeler, S.N. Thai, Y. Cheng, P.J. Horner, D.L. Sellers, S.H. Pun, pH-sensitive polymer micelles provide selective and potentiated lytic capacity to venom peptides for effective intracellular delivery, Biomaterials 192 (2019) 235–244. Epub 2018/11/21. doi:10.1016/j.biomaterials.2018.11.004. PubMed PMID: 30458359; PubMed Central PMCID: PMCPMC6331286.

[6] P. Bilal Ahmad, P. Bilal Ahamad, P. Bilal Ahamad, A. Aqeel, A. Aqeel, K. Javed Masood, et al., The role of the multifunctional antimicrobial peptide melittin in gene delivery, Drug Discov. Today (2021), https://doi.org/10.1016/j.drudis.2021.01.004.

[7] S. Choi, K.D. Lee, Enhanced gene delivery using disulfide-crosslinked low molecular weight polyethylenimine with listeriolysin o-polyethylenimine disulfide conjugate, Journal of Controlled Release 131 (1) (2008) 70–76. Epub 2008/08/12. doi: 10.1016/j.jconrel.2008.07.007. PubMed PMID: 18692533; PubMed Central PMCID: PMCPMC2692728.

[8] N.H. Kim, C. Provoda, K.D. Lee, Design and characterization of novel recombinant listeriolysin O-protamine fusion proteins for enhanced gene delivery, Mol Pharm. 12 (2) (2015) 342–350. Epub 2014/12/19. doi: 10.1021/mp5004543. PubMed PMID: 25521817; PubMed Central PMCID: PMCPMC4319693.

[9] I. Plaza-Ga, V. Manzaneda-González, M. Kisovec, V. Almendro-Vedia, M. Muñoz-Úbeda, G. Anderluh, et al., pH-triggered endosomal escape of pore-forming Listeriolysin O toxin-coated gold nanoparticles, Journal of Nanobiotechnology 17 (1) (2019) 108. Epub 2019/10/19. doi: 10.1186/s12951-019-0543-6. PubMed PMID: 31623647; PubMed Central PMCID: PMCPMC6798460.

[10] D. Scherer, M. Burger, J.C. Leroux, Revival of bioengineered proteins as carriers for nucleic acids, Bioconjug Chem. 35 (5) (2024) 561–566. Epub 2024/04/16. doi: 10.1021/acs.bioconjchem.4c00079. PubMed PMID: 38621363; PubMed Central PMCID: PMCPMC11099893.

[11] N.J. Yang, M.J. Kauke, F. Sun, L.F. Yang, K.F. Maass, M.W. Traxlmayr, et al., Cytosolic delivery of siRNA by ultra-high affinity dsRNA binding proteins, Nucleic Acids Res. 45 (13) (2017) 7602–7614. Epub 2017/06/24. doi:10.1093/nar/gkx546. PubMed PMID: 28641400; PubMed Central PMCID: PMCPMC5570165.

[12] S. Kakimoto, T. Hamada, Y. Komatsu, M. Takagi, T. Tanabe, H. Azuma, et al., The conjugation of diphtheria toxin T domain to poly(ethylenimine) based vectors for enhanced endosomal escape during gene transfection, Biomaterials 30 (3) (2009) 402–408. Epub 2008/10/22. doi: 10.1016/j.biomaterials.2008.09.042. PubMed PMID: 18930314.

[13] S. Kakimoto, T. Tanabe, H. Azuma, T. Nagasaki, Enhanced internalization and endosomal escape of dual-functionalized poly(ethyleneimine)s polyplex with diphtheria toxin T and R domains, Biomedicine & Pharmacotherapy 64 (4) (2010) 296–301. Epub 2010/03/30. doi:10.1016/j.biopha.2009.06.017. PubMed PMID: 20347568.

[14] N. Petrišič, M. Kozorog, S. Aden, M. Podobnik, G. Anderluh, The molecular mechanisms of listeriolysin O-induced lipid membrane damage, Biochim. Biophys. Acta Biomembr. 2021 (7) (1863), 183604. Epub 2021/03/17. doi:10.1016/j.bbamem.2021.183604. PubMed PMID: 33722646.

[15] M.V. Rodnin, V. Vasques-Montes, A. Kyrychenko, N.F.B. Oliveira, M. M. Kashipathy, K.P. Battaile, et al., Histidine protonation and conformational switching in diphtheria toxin translocation domain, Toxins (Basel) 15 (7) (2023). Epub 2023/07/28. doi:10.3390/toxins15070410. PubMed PMID: 37505680; PubMed Central PMCID: PMCPMC10467104.

[16] N.J. Yang, D.V. Liu, D. Sklaviadis, D.Y. Gui, M.G. Vander Heiden, K.D. Wittrup, Antibody-mediated neutralization of perfringolysin o for intracellular protein delivery, Mol Pharm. 12 (6) (2015) 1992–2000. Epub 2015/04/18. doi:10.1021/mp500797n. PubMed PMID: 25881713; PubMed Central PMCID: PMCPMC4876977.

[17] M.E. Lanio, V. Morera, C. Alvarez, M. Tejuca, T. Gomez, F. Pazos, et al., Purification and characterization of two hemolysins from Stichodactyla helianthus, Toxicon 39 (2–3) (2001) 187–194. Epub 2000/09/09. doi:10.1016/s0041-0101(00)00106-9. PubMed PMID: 10978735.

[18] C. Alvarez, F. Pazos, C. Soto, R. Laborde, M.E. Lanio, Pore-forming toxins from sea anemones: from protein-membrane interaction to its implications for developing biomedical applications, in: A. Iglič, M. Rappolt, A.J. García-SÁez (Eds.), Advances in Biomembranes and Lipid Self-Assembly. Advances in Biomembranes and Lipid Self-Assembly vol. 31, Academic Press, 2020, pp. 129–183.

[19] C. Alvarez, J.M. Mancheno, D. Martinez, M. Tejuca, F. Pazos, M.E. Lanio, Sticholysins, two pore-forming toxins produced by the Caribbean Sea anemone Stichodactyla helianthus: their interaction with membranes, Toxicon 54 (8) (2009) 1135–1147. Epub 2009/03/10. doi: 10.1016/j.toxicon.2009.02.022. PubMed PMID: 19268489.

[20] E. Rivera-de-Torre, J. Palacios-Ortega, J.P. Slotte, J.G. Gavilanes, A. Martinez-Del-Pozo, S. Garcia-Linares, Functional and structural variation among sticholysins, pore-forming proteins from the sea anemone *Stichodactyla helianthus*, International Journal of Molecular Sciences 21 (23) (2020). Epub 2020/12/02. doi:10.3390/ijms21238915. PubMed PMID: 33255441; PubMed Central PMCID: PMCPMC7727798.

[21] D. Penton, V. Perez-Barzaga, I. Diaz, M.L. Reytor, J. Campos, R. Fando, et al., Validation of a mutant of the pore-forming toxin sticholysin-I for the construction of proteinase-activated immunotoxins, Protein Engineering, Design & Selection 24 (6) (2011) 485–493. Epub 2011/02/08. doi: 10.1093/protein/gzr002. PubMed PMID: 21296830.

[22] A. Valle, L.B. Perez-Socas, L. Canet, Y.P. Hervis, G. de Armas-Guitart, D. Martins-de-Sa, et al., Self-homodimerization of an actinoporin by disulfide bridging reveals implications for their structure and pore formation, Scientific Reports 8 (1) (2018), 6614. Epub 2018/04/28. doi: 10.1038/s41598-018-24688-2. PubMed PMID: 29700324; PubMed Central PMCID: PMCPMC5920107.

[23] F.W. Studier, Protein production by auto-induction in high density shaking cultures, Protein Expr. Purif. 41 (1) (2005) 207–234. Epub 2005/05/26. doi: 10.1016/j.pep.2005.01.016. PubMed PMID: 15915565.

[24] F. Pazos, A. Valle, D. Martínez, A. Ramírez, L. Calderón, A. Pupo, et al., Structural and functional characterization of a recombinant sticholysin I (rSt I) from the sea anemone Stichodactyla helianthus, Toxicon 48 (8) (2006) 1083–1094. Epub 2006/10/28. doi:10.1016/j.toxicon.2006.09.004. PubMed PMID: 17067649.

[25] Y.P. Hervis, A. Valle, L. Canet, A. Rodríguez, M.E. Lanio, C. Alvarez, et al., Cys mutants as tools to study the oligomerization of the pore-forming toxin sticholysin I, Toxicon 222 (2023) 106994, https://doi.org/10.1016/j.toxicon.2022.106994.

[26] U.K. Laemmli, Cleavage of structural proteins during the assembly of the head of bacteriophage T4, Nature 227 (5259) (1970) 680–685. Epub 1970/08/15. doi: 10.1038/227680a0. PubMed PMID: 5432063.
[27] D. Martinez, A.M. Campos, F. Pazos, C. Alvarez, M.E. Lanio, F. Casallanovo, et al., Properties of St I and St II, two isotoxins isolated from Stichodactyla helianthus: a comparison, Toxicon 39 (10) (2001) 1547–1560. Epub 2001/08/02. doi: 10.1016/s0041-0101(01)00127-1. PubMed PMID: 11478962.
[28] K. Ma, C.L. Mi, X.X. Cao, T.Y. Wang, Progress of cationic gene delivery reagents for non-viral vector, Appl. Microbiol. Biotechnol. 105 (2) (2021) 525–538. Epub 2021/01/05. doi: 10.1007/s00253-020-11028-6. PubMed PMID: 33394152.
[29] F.H. Stephenson, Quantitation of nucleic acids, in: F.H. Stephenson (Ed.), Calculations for Molecular Biology and Biotechnology, Academic Press, Burlington, 2003, pp. 90–108.
[30] A. Mann, G. Thakur, V. Shukla, A.K. Singh, R. Khanduri, R. Naik, et al., Differences in DNA condensation and release by lysine and arginine homopeptides govern their DNA delivery efficiencies, Mol. Pharm. 8 (5) (2011) 1729–1741. Epub 2011/07/26. doi: 10.1021/mp2000814. PubMed PMID: 21780847.
[31] T. Xu, W. Liu, S. Wang, Z. Shao, Elucidating the role of free polycationic chains in polycation gene carriers by free chains of polyethylenimine or N,N,N-trimethyl chitosan plus a certain polyplex, International Journal of Nanomedicine 9 (2014) 3231–3245. Epub 2014/07/26. doi: 10.2147/IJN.S64308. PubMed PMID: 25061299; PubMed Central PMCID: PMCPMC4086671.
[32] S. Bolte, F.P. Cordelières, A guided tour into subcellular colocalization analysis in light microscopy, J. Microsc. 224 (Pt 3) (2006) 213–232. Epub 2007/01/11. doi: 10.1111/j.1365-2818.2006.01706.x. PubMed PMID: 17210054.
[33] J.P. Tam, C.R. Wu, W. Liu, Zhang JWJJotACS., Disulfide bond formation in peptides by dimethyl sulfoxide, Scope and Applications. 113 (17) (1991) 6657–6662.
[34] C.G. Victorio, N. Sawyer, Folding-assisted peptide disulfide formation and dimerization, ACS Chem. Biol. 18 (7) (2023) 1480–1486. Epub 2023/06/30. doi: 10.1021/acschembio.3c00268. PubMed PMID: 37390465.
[35] M. Tejuca, M. Dalla Serra, C. Potrich, C. Alvarez, G. Menestrina, Sizing the radius of the pore formed in erythrocytes and lipid vesicles by the toxin sticholysin I from the sea anemone Stichodactyla helianthus, J. Membr. Biol. 183 (2) (2001) 125–135. Epub 2001/09/20. doi: 10.1007/s00232-001-0060-y. PubMed PMID: 11562794.
[36] H.J. Park, B. Park, S.S. Lee, Radiomics and deep learning: hepatic applications, Korean Journal of Radiology 21 (4) (2020) 387–401. Epub 2020/03/21. doi: 10.3348/kjr.2019.0752. PubMed PMID: 32193887; PubMed Central PMCID: PMCPMC7082656.
[37] J. Schindelin, I. Arganda-Carreras, E. Frise, V. Kaynig, M. Longair, T. Pietzsch, et al., Fiji: an open-source platform for biological-image analysis, Nature Methods 9 (7) (2012) 676–682. Epub 2012/06/30. doi: 10.1038/nmeth.2019. PubMed PMID: 22743772; PubMed Central PMCID: PMCPMC3855844.
[38] S. Falke, C. Betzel, Dynamic light scattering (DLS), in: A.S. Pereira, P. Tavares, P. Limão-Vieira (Eds.), Radiation in Bioanalysis, Springer International Publishing, Cham, 2019, pp. 173–193.
[39] K.W. Dunn, M.M. Kamocka, J.H. McDonald, A practical guide to evaluating colocalization in biological microscopy, American Journal of Physiology Cell Physiology 300 (4) (2011). C723-42. Epub 2011/01/07. doi:10.1152/ajpcell.00462.2010. PubMed PMID: 21209361; PubMed Central PMCID: PMCPMC3074624.
[40] M.S. Al-Dosari, X. Gao, Nonviral gene delivery: principle, limitations, and recent progress, AAPS J 11 (4) (2009) 671–681. Epub 2009/10/17. doi:10.1208/s12248-009-9143-y. PubMed PMID: 19834816; PubMed Central PMCID: PMCPMC2782077.
[41] N. Bono, F. Ponti, D. Mantovani, G. Candiani, Non-viral in vitro gene delivery: it is now time to set the bar!, Pharmaceutics 12 (2) (2020). Epub 2020/02/27. doi: 10.3390/pharmaceutics12020183. PubMed PMID: 32098191; PubMed Central PMCID: PMCPMC7076396.
[42] H. Zu, D. Gao, Non-viral vectors in gene therapy: recent development, challenges, and prospects, AAPS J 23 (4) (2021) 78. Epub 2021/06/03. doi:10.1208/s12248-021-00608-7. PubMed PMID: 34076797; PubMed Central PMCID: PMCPMC8171234.
[43] I.M.S. Degors, C. Wang, Z.U. Rehman, I.S. Zuhorn, Carriers break barriers in drug delivery: endocytosis and endosomal escape of gene delivery vectors, Accounts of Chemical Research 52 (7) (2019) 1750–1760. Epub 2019/06/28. doi: 10.1021/acs.accounts.9b00177. PubMed PMID: 31243966; PubMed Central PMCID: PMCPMC6639780.
[44] X. Bi, J. Yin, D. Zhang, X. Zhang, S. Balamkundu, J. Lescar, et al., Tagging transferrin receptor with a disulfide FRET probe to gauge the redox state in endosomal compartments, Anal. Chem. 92 (18) (2020) 12460–12466. Epub 2020/07/21. doi:10.1021/acs.analchem.0c02264. PubMed PMID: 32686399.
[45] K. Dutta, R. Das, J. Medeiros, S. Thayumanavan, Disulfide bridging strategies in viral and nonviral platforms for nucleic acid delivery, Biochemistry 60 (13) (2021) 966–990. Epub 2021/01/12. doi:10.1021/acs.biochem.0c00860. PubMed PMID: 33428850; PubMed Central PMCID: PMCPMC8753971.
[46] G. Saito, G.L. Amidon, K.D. Lee, Enhanced cytosolic delivery of plasmid DNA by a sulfhydryl-activatable listeriolysin O/protamine conjugate utilizing cellular reducing potential, Gene Ther. 10 (1) (2003) 72–83. Epub 2003/01/15. doi: 10.1038/sj.gt.3301859. PubMed PMID: 12525839.
[47] M. Mannisto, S. Vanderkerken, V. Toncheva, M. Elomaa, M. Ruponen, E. Schacht, et al., Structure-activity relationships of poly(L-lysines): effects of pegylation and molecular shape on physicochemical and biological properties in gene delivery, J. Control. Release 83 (1) (2002) 169–182. Epub 2002/09/11. doi:10.1016/s0168-3659(02)00178-5. PubMed PMID: 12220848.
[48] T. Arakawa, Y. Kita, S.N. Timasheff, Protein precipitation and denaturation by dimethyl sulfoxide, Biophys. Chem. 131 (1–3) (2007) 62–70. Epub 2007/10/02. doi:10.1016/j.bpc.2007.09.004. PubMed PMID: 17904724.
[49] M. Jackson, H.H. Mantsch, Beware of proteins in DMSO, Biochim. Biophys. Acta 1078 (2) (1991) 231–235. Epub 1991/06/24. doi:10.1016/0167-4838(91)90563-f. PubMed PMID: 2065090.
[50] G. Anderluh, P. Macek, Cytolytic peptide and protein toxins from sea anemones (Anthozoa: Actiniaria), Toxicon 40 (2) (2002) 111–124. Epub 2001/11/02. doi: 10.1016/s0041-0101(01)00191-x. PubMed PMID: 11689232.
[51] C. Alvarez, I.F. Pazos, M.E. Lanio, D. Martinez, S. Schreier, F. Casallanovo, et al., Effect of pH on the conformation, interaction with membranes and hemolytic activity of sticholysin II, a pore forming cytolysin from the sea anemone Stichodactyla helianthus, Toxicon 39 (4) (2001) 539–553. Epub 2000/10/12. doi: 10.1016/s0041-0101(00)00166-5. PubMed PMID: 11024494.
[52] C.A. Valcarcel, M. Dalla Serra, C. Potrich, I. Bernhart, M. Tejuca, D. Martinez, et al., Effects of lipid composition on membrane permeabilization by sticholysin I and II, two cytolysins of the sea anemone *Stichodactyla helianthus*, Biophysical Journal 80 (6) (2001) 2761–2774. Epub 2001/05/24. doi: 10.1016/S0006-3495(01)76244-3. PubMed PMID: 11371451; PubMed Central PMCID: PMCPMC1301462.
[53] L.M. Hellman, M.G. Fried, Electrophoretic mobility shift assay (EMSA) for detecting protein-nucleic acid interactions, Nature Protocols 2 (8) (2007) 1849–1861. Epub 2007/08/19. doi: 10.1038/nprot.2007.249. PubMed PMID: 17703195; PubMed Central PMCID: PMCPMC2757439.
[54] T. Zhou, A. Llizo, C. Wang, G. Xu, Y. Yang, Nanostructure-induced DNA condensation, Nanoscale 5 (18) (2013) 8288–8306. Epub 2013/07/11. doi: 10.1039/c3nr01630g. PubMed PMID: 23838744.